Am J Cancer Res 2020;10(11):3666-3685
www.ajcr.us /ISSN:2156-6976/ajcr0120172

Original Article

Chiauranib selectively inhibits colorectal cancer with *KRAS* wild-type by modulation of ROS through activating the p53 signaling pathway

Haofan Yin[1*], Jinye Xie[3*], Ping Jiang[5*], Xi Jiang[1], Deyu Duan[1], Junhua Qi[1], Zhaofan Luo[1], Caiqi Ma[4], Honghai Hong[2]

[1]Department of Clinical Laboratory, The Seventh Affiliated Hospital of Sun Yat-sen University, Shenzhen, Guangdong, China; [2]Department of Clinical Laboratory, The Third Affiliated Hospital of Guangzhou Medical University, Guangzhou, Guangdong, China; [3]Department of Laboratory Medicine, Zhongshan People's Hospital, Zhongshan, Guangdong, China; [4]Reproductive Medical Center, Guangzhou Women and Children's Medical Center of Sun Yat-sen University, Guangzhou, Guangdong, China; [5]Department of Clinical Medical Laboratory, Guangzhou First' People Hospital, School of Medicine, South China University of Technology, Guangzhou, Guangdong, China. [*]Equal contributors.

Received August 12, 2020; Accepted October 21, 2020; Epub November 1, 2020; Published November 15, 2020

Abstract: Colorectal cancer (CRC) is one of the top three most deadly cancers despite using chemotherapy based on oxaliplatin or irinotecan combined with targeted therapy. Chiauranib has recently been identified to be a promising anticancer candidate with impressive efficacy and safety. However, the role and molecular mechanisms of Chiauranib in the treatment of CRC remain to be elucidated. Our study shows that Chiauranib inhibits cell proliferation and induces apoptosis in *KRAS* wild-type CRC cells in a dose- and time-dependent manner, but not mutation ones. Meanwhile, Chiauranib increases ROS production in *KRAS* wild-type CRC cells. Moreover, Chiauranib selectively suppresses *KRAS* wild-type CRC cells growth *in vivo*. Mechanistically, Chiauranib inhibits *KRAS* wild-type CRC cells by triggering ROS production via activating the p53 signaling pathway. Further, *KRAS* mutation CRC cells are resistant to Chiauranib by increasing Nrf2 to stably elevate the basal antioxidant program and thereby lower intracellular ROS induced by Chiauranib. Our findings provide the rationale for further clinical evaluation of Chiauranib as a therapeutic agent in treating *KRAS* wild-type CRC.

Keywords: Colorectal cancer, chiauranib, ROS

Introduction

Colorectal cancer (CRC) ranks as the third leading cause of cancer death worldwide [1]. Despite the emergence of numerous screening methods to reduce CRC incidence, an increasing proportion of CRC patients are diagnosed at an advanced stage, which results in difficulties in curative removal of primary tumors and metastases [2]. For those patients, irinotecan- or oxaliplatin-based chemotherapy combined with targeted therapy are the leading strategies in suppressing the further growth and spread, and even killing the cancer cells [3]. However, these chemotherapies are associated with unsatisfying response rate, systemic toxicity, and acquired resistance [4]. Moreover, one of the most breakthrough targeted therapy anti-EGFR compounds are limited to being used in *EGFR*- and *KRAS*-wildtype otherwise in CRC patients with those drug-resistant mutation [5-7]. Therefore, more investments are urgent to be pledged to develop novel targets and agents.

Chiauranib is a novel oral multi-target small molecule inhibitor of select serine threonine-kinases, including the angiogenesis-related kinases (VEGFR1, VEGFR2, VEGFR3, and c-Kit), the chronic inflammation-related kinase CSF-1R, and the mitosis-related kinase Aurora B, with a variety of potential anti-tumor activities [8-10]. Chiauranib reduces hepatocellular carcinoma and gastric cancer cell proliferation by simultaneous inhibiting VEGFR2 and Aurora B [8]. Besides, Chiauranib exerts anti-tumor

effect against angiogenesis and mitosis in hematologic tumors, such as acute myeloid leukemia and Non-Hodgkin's lymphomas [9, 10]. The animal study results illustrate that Chiauranib has impressive efficacy and safety, verified in a phase I clinical trial (NCT03074-825) [10, 11]. Currently, Chiauranib phase Ib/II clinical trials are undergoing in multiply cancers. However, the efficacy and potential mechanism of Chiauranib in the treatment of CRC have not been investigated.

Reactive oxygen species (ROS) are essential signaling messengers of normal cells and tumor cells [12]. Moderate levels of ROS contribute to tumor development, promoting cell differentiation, activating cancer angiogenesis, and metastasis. But excessive oxidative stress causes DNA damage and abnormal stress response, thus triggering cancer cell death [13, 14]. Therefore, it might be effective to eliminate cancer cells by increasing ROS generation. Cellular redox state can be modulated by the tumor suppressor protein p53, which is an essential regulator of the DNA damage response, cell cycle, and cell apoptosis [15]. The p53 protein is tightly regulated by post-transcriptional modifications such as phosphorylation and ubiquitination [16]. Chiauranib has been reported to regulate p53 phosphorylation by inhibiting Aurora B activity [17]. However, whether Chiauranib can induce ROS is still unclear.

Our results demonstrated the anti-tumor role of Chiauranib in inhibition of cell proliferation and induction of cell apoptosis in *KRAS*-wildtype CRC by triggering ROS production through activating the p53 signaling pathway, indicating that Chiauranib may be a promising novel strategy to treat *KRAS*-wildtype CRC.

Materials and methods

Cell lines and culture

The human CRC cell lines (SW48, $CaCO_2$, LoVo, HCT116) were obtained from the American Type Culture Collection (Manassas, USA). Cell lines were authenticated by Cellcook Biotech Co., Ltd, (Guangzhou, China). SW48 $KRAS^{WT}$, SW48 $KRAS^{G13D}$, LoVo-shNC and LoVo-shKRAS cells were previous constructed [18]. All these cells were cultured in RPMI1640 (Gibco, New York, USA, Cat. No. 61870044) and supplemented with 10% FBS (Gibco, Uruguay, 10270-106) at 37°C in a humidified incubator containing 5% CO_2.

Western blotting

Western blotting was performed according to a standard protocol, as described previously [19]. The total proteins were collected using SDS lysis buffer (Beyotime, P0013G), and protein concentration were determined by Bicinchoninic Acid (KeyGen, KGP902). Nuclear extracts were obtained using the NE-PER Nuclear and cytoplasmic extraction reagents (Thermo Scientific, Massachusetts, USA, 78833) according to the manufacturer's instructions. The following primary antibodies were used: CDK1 (AF1516), P21 (AP021) from Beyotime (Shanghai, China); Bcl-2 (sc-7382), Bax (sc-6236) from Santa Cruz (California, USA); P53 (CBL404) from Merck Millipore (Boston, USA); Aurora B (ab2254), p-Aurora B (ab115793), KRAS (ab180772), Nrf2 (ab-31163) from Abcam (Cambridge, UK); β-actin (A5441) from Sigma-Aldrich (St. Louis, USA). HRP-conjugated anti-rabbit IgG (Cell Signaling Tech, #7074) and anti-mouse IgG (Sigma-Aldrich, AP308P) were used as secondary antibodies. Proteins were determined using ECL Plus Reagent (Millipore, WBKLS0100).

RNA isolation and RT-qPCR

Total RNA was extracted using TRIzol (Thermo Scientific, 15596026) according to the manufacturer's protocol [19]. First-strand cDNA synthesis was performed using 500 nanograms of total RNA, and the RT-qPCR analysis system was performed using iQ SYBR Green Supermix and the iCycler Real-time PCR Detection System (Bio-Rad, USA). β-actin was used for normalization. The PCR primer sequences are listed in Supplementary Table 1.

Immunofluorescence staining

After fixed in 4% paraformaldehyde, cells were blocked with goat serum at 37°C for 1 h. They were incubated with rabbit Ki67 (Millipore, AB9260) antibodies at 4°C overnight, then were incubated with FITC conjugated goat anti-rabbit IgG (Dako, Glostrup, Denmark, K500711) at 37°C for 1 h after three times washing. Finally, the cell nucleus was stained with DAPI (Sigma-Aldrich, D9542).

Cell counting Kit-8 (CCK8)

Cell proliferation was measured via cell viability with a Cell Counting Kit-8 (Dojindo, Japan). CRC cells were seeded into 96-well plates and cultured for 24, 48 and 72 h. Then, 100 μl CCK8 reagent was added to 96-well plates and incubated for 2 h. The absorbance (OD450 nm) was measured using a microplate reader (TECAN, Switzerland) and calculated.

Colony formation assay

CRC cells were plated in 6-well dishes (500 cell/dish) and then incubated for 2 weeks for colony formation with or without Chiauranib. After 14 days, cell colonies were then fixed in 4% polyformaldehyde and stained with 0.1% crystal violet. All colonies were counted separately for each sample, and the relative colony numbers were calculated.

Dihydroethidium (DHE) staining

Reactive oxygen species (ROS) were measured with DHE staining following incubation at 37°C for 30 min (Beyotime, Shanghai, China). PBS was used instead of DHE in the negative control group. The fluorescence intensity was quantified with the ImageJ software program (National Institutes of Health, Bethesda, MD, USA).

Terminal deoxynucleotidyl transferase mediated dUTP nick end labeling (TUNEL) staining

Tissue sections were deparaffinized and hydrated in xylene and gradient concentrations of ethanol, then incubated in proteinase K at room temperature for 30 min and stained with TUNEL kit (Sigma-Aldrich, St. Louis, MO, USA). Label solution was used instead of TUNEL reagent in the negative control group. All the images were captured by a fluorescence microscope (DFC700T, Leica, Germany). Cells that were positive for TUNEL staining and aligned with DAPI staining were considered apoptotic cells and counted.

Annexin V/propidium iodide flow cytometric analysis

CRC cell staining with Annexin V and PI was carried out using an Annexin V-FITC/PI Apoptosis Detection kit (Merck, Germany). A total of 1×10^6 cells were incubated at 37°C for 30 minutes before centrifugation to collect the cell pellet, then resuspended in a Ca^{2+}-enriched binding buffer and analysed using a Beckman Coulter flow cytometry. Data were calculated using CellQuest software.

ROS assays

Cells were plated at a density of 200000 cells per well in 12-well plates. After 48 hours, DCF-DA (Sigma) and MitoSOX (Invitrogen) was added to each well at a concentration of 5 μM. After 30 min, the samples were run on the flow cytometer to detect fluorescence. Each sample was collected using 20,000 events.

Tumor xenograft

Male BALB/c nude mice (4-weeks-old, 16-18 g) were purchased from Beijing Vital River Laboratory Animal Technology Co., Ltd. (Beijing, China). Based on a previously described standard protocol, the mice were randomly divided into the indicated groups. 1×10^6 SW48 or LoVo cells were inoculated into the inguinal folds of mice (n = 8 in each cell line per group). Tumor volumes were measured with an external caliper, and calculated according to the following formula: Volume = length × width^2/2. At 27 days after inoculation, the mice were sacrificed, and the tumors were dissected, weighed, taken photos, and stored at -80°C for further experiments.

siRNA and transfection

P53 siRNA, Nrf2 siRNA and control siRNA were purchased from RiboBio (Guangzhou, China). According to the manufacturer's instructions, transfections were performed at approximately 60% confluency using RNAiMAX (Invitrogen, USA). After 48 hours, confirmation of interference was carried out using real-time quantitative PCR (RT-qPCR) and Western blotting.

RNA-Seq

RNA sequence was performed with BGISEQ-500 platform. In brief, the first step in the workflow involved purifying the poly-A containing mRNA molecules using poly-T oligo-attached magnetic beads. Following purification, the mRNA was fragmented into small pieces using

divalent cations under elevated temperature. The cleaved RNA fragments were copied into first strand cDNA using reverse transcriptase and random primers. This was followed by second strand cDNA synthesis using DNA Polymerase I and RNase H. These cDNA fragments then had the addition of a single 'A' base and subsequent ligation of the adapter. The products were then purified and enriched with PCR amplification. We then quantified the PCR yield by Qubit and pooled samples together to make a single strand DNA circle (ssDNA circle), which gave the final library. DNA nanoballs (DNBs) were generated with the ssDNA circle by rolling circle replication (RCR) to enlarge the fluorescent signals at the sequencing process. The DNBs were loaded into the patterned nanoarrays and single-end read of 50 bp were read through on the BGISEQ-500 platform for the following data analysis study. For this step, the BGISEQ-500 platform combined the DNA nanoball-based nanoarrays and stepwise sequencing using Combinational Probe-Anchor Synthesis Sequencing Method. Tools such as HISAT2, Bowtie2, Cluster etc. were used for the following bioinformatics analysis. In the analysis of differentially expressed genes (DEGs), the genes that had more than double fold change and the corrected *P* value is less than or equal to 0.05 were defined as DEGs. With DEGs, we performed KEGG pathway classification and Gene set enrichment analysis (GSEA) using R. we have upload the sequence data onto the online database SRA (Sequence Read Archieve). Our sequence data is numbered PRJNA667187.

Statistical analysis

The variability of the data is presented as the SD (mean ± SD) and was assessed with Student's *t* test between two groups. For multiple groups, significant differences were determined using one-way ANOVA. Statistical significance was defined at $P < 0.05$.

Results

The anti-tumor effect of Chiauranib in KRAS wild-type CRC cells

To validate whether Chiauranib exhibited an anti-tumor effect against CRC, CCK-8 assays were performed to evaluate the cell viability in response to Chiauranib treatment in different human CRC cell lines (LoVo, HCT116, SW48, $CaCO_2$). Surprisingly, Chiauranib treatment markedly decreased the cell viability of SW48 and $CaCO_2$ in a concentration- and time-dependent manner, whereas LoVo and HCT116 cells were resistant to Chiauranib (**Figure 1A**, **1B**). The IC50 values of Chiauranib in SW48 cells and $CaCO_2$ cells were 8.843 μM and 9.165 μM, respectively (**Figure 1C**). Chemotherapeutic drug resistance often occurred in CRC, especially those with genetic mutations of *KRAS*, *BRAF*, *TP53*, *PIK3CA*. There was only *KRAS* gene mutation in LoVo cells, which also occurred in HCT116 cells [20]. Meanwhile, both SW48 and $CaCO_2$, which sensitive to Chiauranib, were *KRAS* wild-type cells [20]. Consequently, we investigated whether Chiauranib resistance of LoVo and HCT116 cells was related to *KRAS* mutations? We established SW48 $KRAS^{G13D}$ cell model by the CRISPR-Cas9 system as previously described [18], and the results indicated that *KRAS* mutations could impair the sensitivity to the anti-viability therapy of Chiauranib (**Figure 1D**, **1F**). On the contrary, short hairpin RNA (shRNA)-mediated *KRAS* knockdown up-regulated the sensitivity to Chiauranib in LoVo cells (**Figure 1E**, **1G**). Taken together, these results suggested that Chiauranib exhibited a great concentration- and time-dependent antitumor effect against *KRAS* wild-type CRC cells.

Chiauranib selectively inhibits KRAS wild-type CRC cells proliferation

Colony formation and EdU assays were performed to further validate the cytotoxic effects of Chiauranib towards CRC cells on proliferation. As shown in **Figure 2A**, **2B**, Chiauranib concentration-dependently impaired the cloning ability of *KRAS* wild-type and *KRAS* knockdown CRC cells, whereas the phenomenon did not occur in *KRAS* mutation cells. Consistently, EdU experiments showed that the proliferation of SW48 $KRAS^{WT}$ and LoVo-shKRAS cells was significantly inhibited under Chiauranib treatment for 48 hours, an effect not seen in *KRAS* mutation cells SW48 $KRAS^{G13D}$ and LoVo-shNC (**Figure 2C**, **2D**). These results indicated that Chiauranib selectively inhibited *KRAS* wild-type CRC cells proliferation.

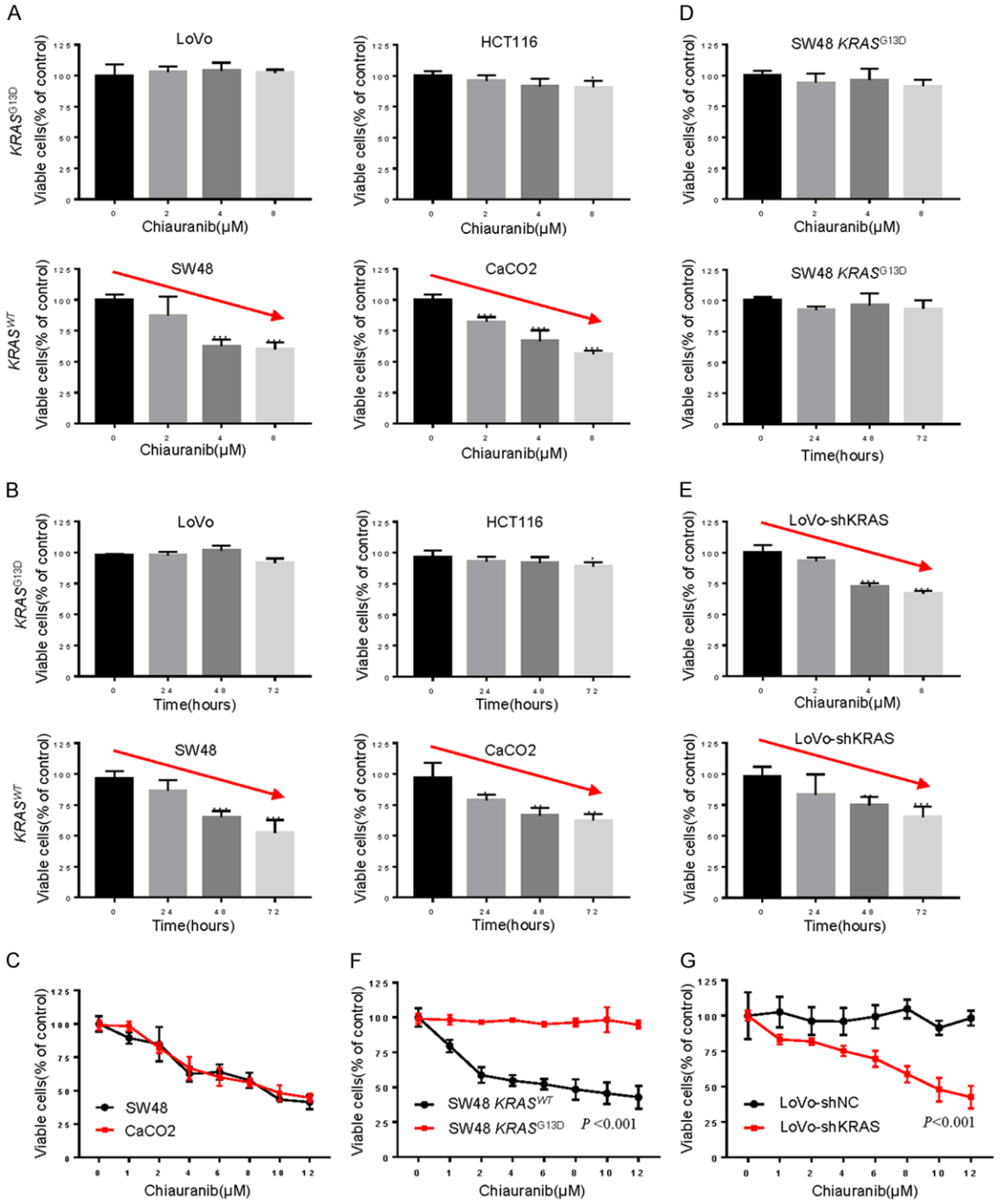

Figure 1. The anti-tumor effect of Chiauranib in *KRAS* wild-type CRC cells. A. 48-hour cell viability of *KRAS*^{WT} CRC cell lines SW48 and $CaCO_2$, *KRAS*^{G13D} CRC cell lines LoVo and HCT116 were detected by CCK-8 after treatment with 0, 2, 4, 8 μM Chiauranib; ***P < 0.001 was compared with 0 μM Chiauranib. B. Cell viability of *KRAS*^{WT} CRC cell lines SW48 and $CaCO_2$, *KRAS*^{G13D} CRC cell lines LoVo and HCT116 were detected by CCK-8 after treatment with 4 μM Chiauranib for 0, 24, 48, 72 hours; *P < 0.05, **P < 0.01 and ***P < 0.001 was compared with 0 hours. C. 48-hour cell viability of SW48 and $CaCO_2$ cells were detected by CCK-8 after treatment with 0, 1, 2, 4, 8, 10, 12 μM Chiauranib. D. SW48 *KRAS*^{G13D} cells viability were determined after treatment with incremental Chiauranib for 48 hours and treatment with 4 μM Chiauranib for 0, 24, 48, 72 hours. E. LoVo-shKRAS cells viability were determined after treatment with incremental Chiauranib for 48 hours and treatment with 4 μM Chiauranib for 0, 24, 48, 72 hours; **P < 0.01, ***P < 0.001. F. 48-hour cell viability of SW48 *KRAS*^{WT} and SW48 *KRAS*^{G13D} were determined after treatment with incremental Chiauranib; ***P < 0.001 was compared with *KRAS*^{WT} SW48 group. G. 48-hour cell viability of LoVo-shNC and LoVo-shKRAS were determined after treatment with incremental Chiauranib; ***P < 0.001 was compared with LoVo-shNC group. All Bars represented the mean ± SD of three independent experiments.

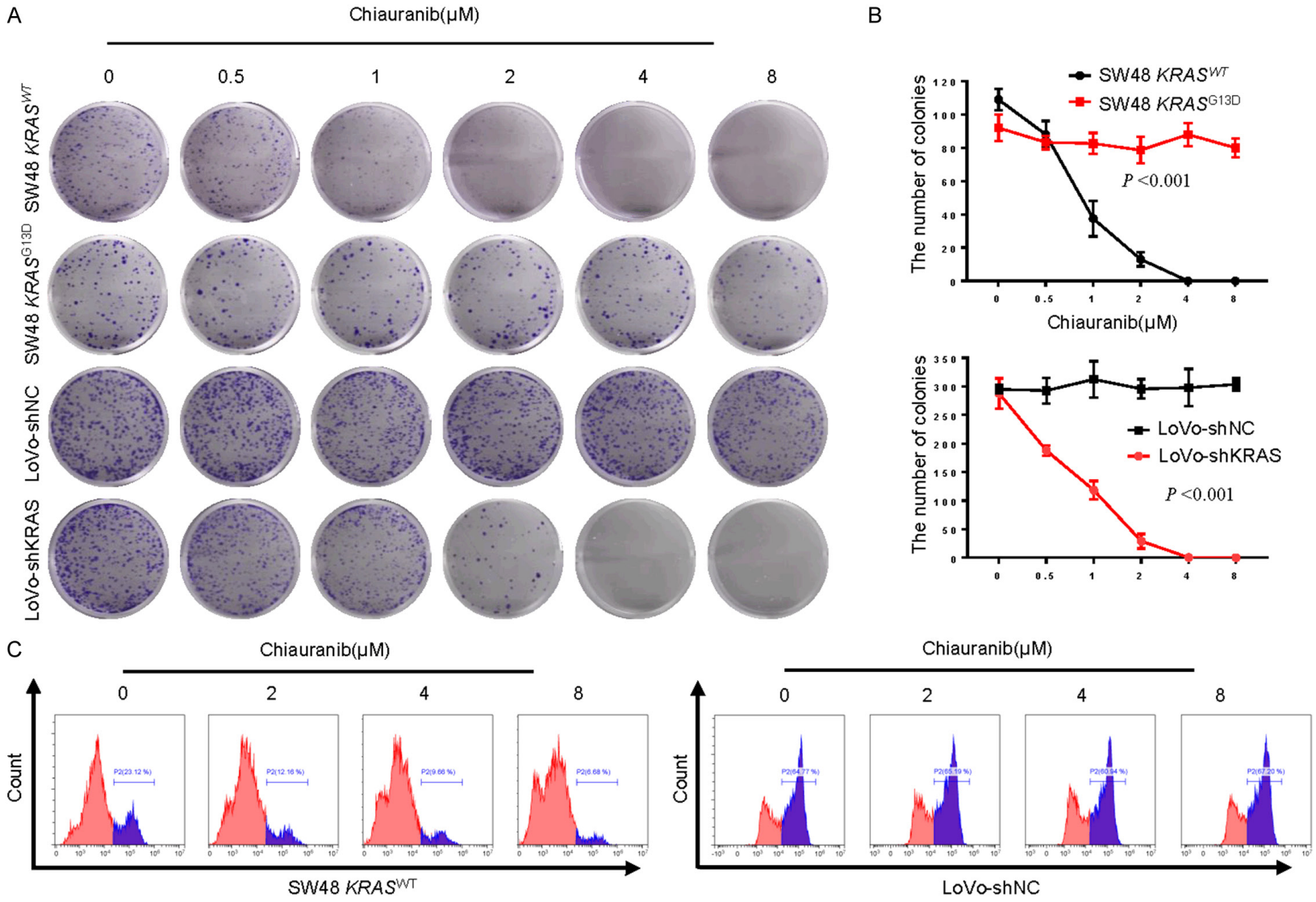
A
Chiauranib(μM)
0
0.5
1
2
4
8
SW48 KRASWT
SW48 KRASG13D
LoVo-shNC
LoVo-shKRAS
B
SW48 KRASWT
SW48 KRASG13D
The number of colonies
P <0.001
Chiauranib(μM)
LoVo-shNC
LoVo-shKRAS
P <0.001
C
Chiauranib(μM)
0
2
4
8
Count
SW48 KRASWT
Chiauranib(μM)
LoVo-shNC

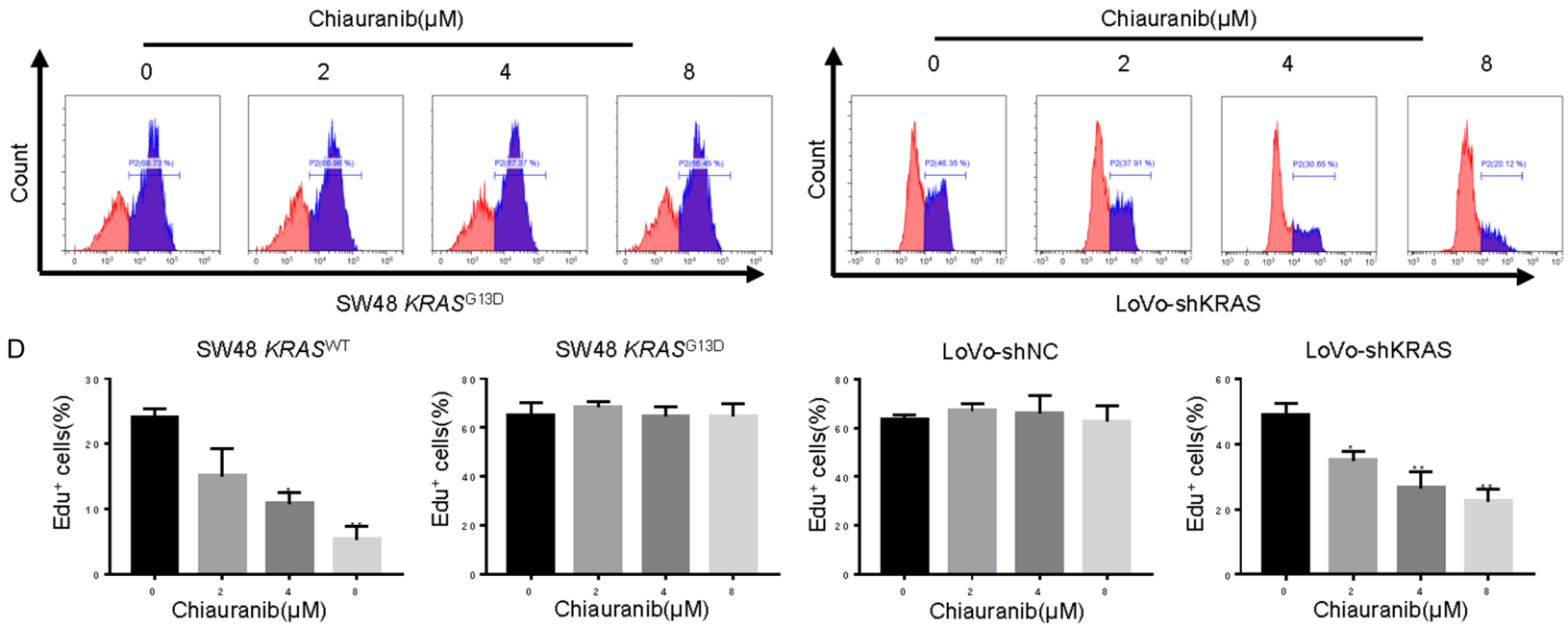

Figure 2. Chiauranib selectively inhibits *KRAS* wild-type CRC cells proliferation. A. Representative images of colony formation in the indicated $KRAS^{WT}$ SW48, $KRAS^{G13D}$ SW48, LoVo-shNC and LoVo-shKRAS cells after treatment with 0, 0.5, 1, 2, 4, 8 μM Chiauranib for 14 days. B. Statistical analysis of colony formation. Bars represent the mean ± SD of three independent experiments; $***P < 0.001$ was compared with $KRAS^{WT}$ SW48 group or LoVo-shNC group. C. Representative images of EDU staining in the indicated cells after treatment with 0, 2, 4, 8 μM Chiauranib for 48 hours. D. Statistical analysis of EDU staining. Bars represented the mean ± SD of three independent experiments; $*P < 0.05$, $**P < 0.01$ was compared with 0 μM Chiauranib.

Chiauranib selectively promotes KRAS wild-type CRC cells apoptosis

Previous studies have suggested that Chiauranib exerted anti-tumor activity by inducing apoptosis [9, 10]. To evaluate whether apoptosis was involved in Chiauranib-induced cytotoxicity in CRC cells, apoptosis was determined by flow cytometric analysis with Annexin V/propidium iodide (PI) double staining. As expected, Chiauranib apparently increased the apoptosis rate in *KRAS* wild-type and *KRAS* knockdown CRC cells, whereas Chiauranib did not affect *KRAS* mutation cells apoptosis (**Figure 3A**, **3B**). The pro-apoptotic effect of Chiauranib in CRC cells was further evidenced by TUNEL staining. Our results showed that the TUNEL staining intensity was significantly increased in SW48 $KRAS^{WT}$ and LoVo-shKRAS cells, and the phenomenon did not occur in *KRAS* mutation cells SW48 $KRAS^{G13D}$ and LoVo-shNC (**Figure 3C**, **3D**). Collectively, these results demonstrated that Chiauranib exhibited a pro-apoptotic effect in *KRAS* wild-type CRC cells.

Chiauranib alters gene sets related to ROS in KRAS wild-type CRC cells

To demonstrate the molecular mechanisms of Chiauranib-induced CRC suppression, we determined the global gene expression pattern for Chiauranib-treated SW48 cell and compared it with that for the controls based on RNA-Seq analysis. Using a ≥ 2-fold change (FC) and < 0.05 *P*-value as a cut-off, we identified a series of differential expressed genes (DEGs) when compared between Chiauranib-treated and control groups (Supplementary Figure 1). Furthermore, KEGG pathway analysis presented that these DEGs mainly participated in the p53 signaling pathway (**Figure 4A**). Consistently, gene set enrichment analysis (GSEA) revealed that these DEGs were enriched in oxidative phosphorylation and p53 signaling pathway (**Figure 4B**; Supplementary Figure 2). Meanwhile, the heat map demonstrated 44 DEGs related to oxidative phosphorylation and p53 signaling pathway (**Figure 4C**). To verify the accuracy of the RNA-Seq, we selected nine essential p53 signaling pathway-related genes for Q-PCR validation, including *BCL2*, *BAX*, *ZMAT3*, *FAS*, *TP53AIP1*, *CDKN1A*, *CDK1*, *EI24* and *MDM2* (**Figure 4D**). The results revealed that the changes in the nine genes were consistent with the sequencing results.

Previous studies have proven that activation of the p53 signaling pathway led to imbalance of oxidative phosphorylation, thus inducing ROS production [21]. ROS accumulation could inhibit cell proliferation and induce cell apoptosis. Therefore, we determined to detect whether Chiauranib increased intracellular ROS levels. The results showed that Chiauranib treatment markedly increased MitoSOX fluorescence (for mitochondrial $O_2^{\bullet-}$) and DCF-DA fluorescence (for H_2O_2) of SW48 $KRAS^{WT}$ and LoVo-shKRAS cells, but not mutation ones (**Figure 4E**, **4F**; Supplementary Figure 3). Taken together, these observations indicated that Chiauranib increased the level of ROS in *KRAS* wild-type CRC cells.

Chiauranib induces ROS of KRAS wild-type CRC cells by activating the p53 signaling pathway

In the above study, RNA-Seq analysis indicated that Chiauranib significantly activated the p53 signaling pathway. To further explore the mechanism of Chiauranib activating the p53 signaling pathway in *KRAS* wild-type CRC cells, we detected a series of critical molecules in the p53 signaling pathway. The mRNA and protein levels of these downstream molecules in the p53 signaling pathway were substantially changed. However, the transcription level of p53 did not change, but the protein level increased significantly, indicating that Chiauranib might affect the post-transcriptional regulation of p53. It has been reported that Chiauranib could inhibit the phosphorylation of Aurora B, which participated in regulating p53 phosphorylation [8]. Indeed, our results showed that Chiauranib could inhibit Aurora B phosphorylation in *KRAS* wild-type CRC cells, thus inducing p53 increasing (**Figure 5A**). Silencing p53 inhibited the p53 signaling pathway activated by Chiauranib, while it did not affect the phosphorylation of Aurora B (**Figure 5B**, **5C**). These results indicated that Chiauranib inhibited Aurora B phosphorylation, resulting in an increased in p53 expression.

Next, we investigated whether ROS accumulation caused by Chiauranib was through activa-

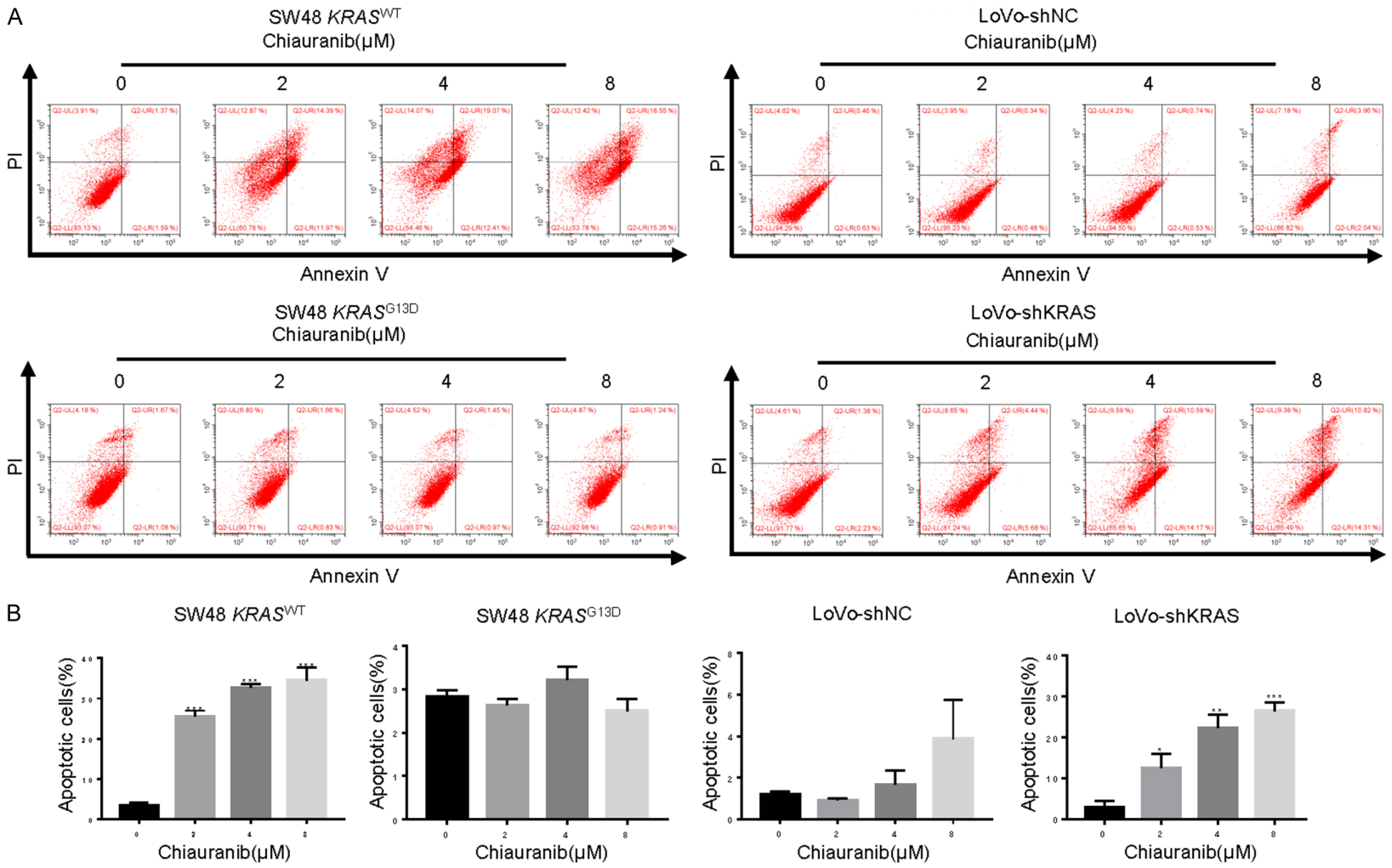
A
SW48 KRASWT
Chiauranib(μM)
0
2
4
8
PI
Annexin V
LoVo-shNC
Chiauranib(μM)
SW48 KRASG13D
Chiauranib(μM)
LoVo-shKRAS
Chiauranib(μM)
B
SW48 KRASWT
SW48 KRASG13D
LoVo-shNC
LoVo-shKRAS
Apoptotic cells(%)
Chiauranib(μM)

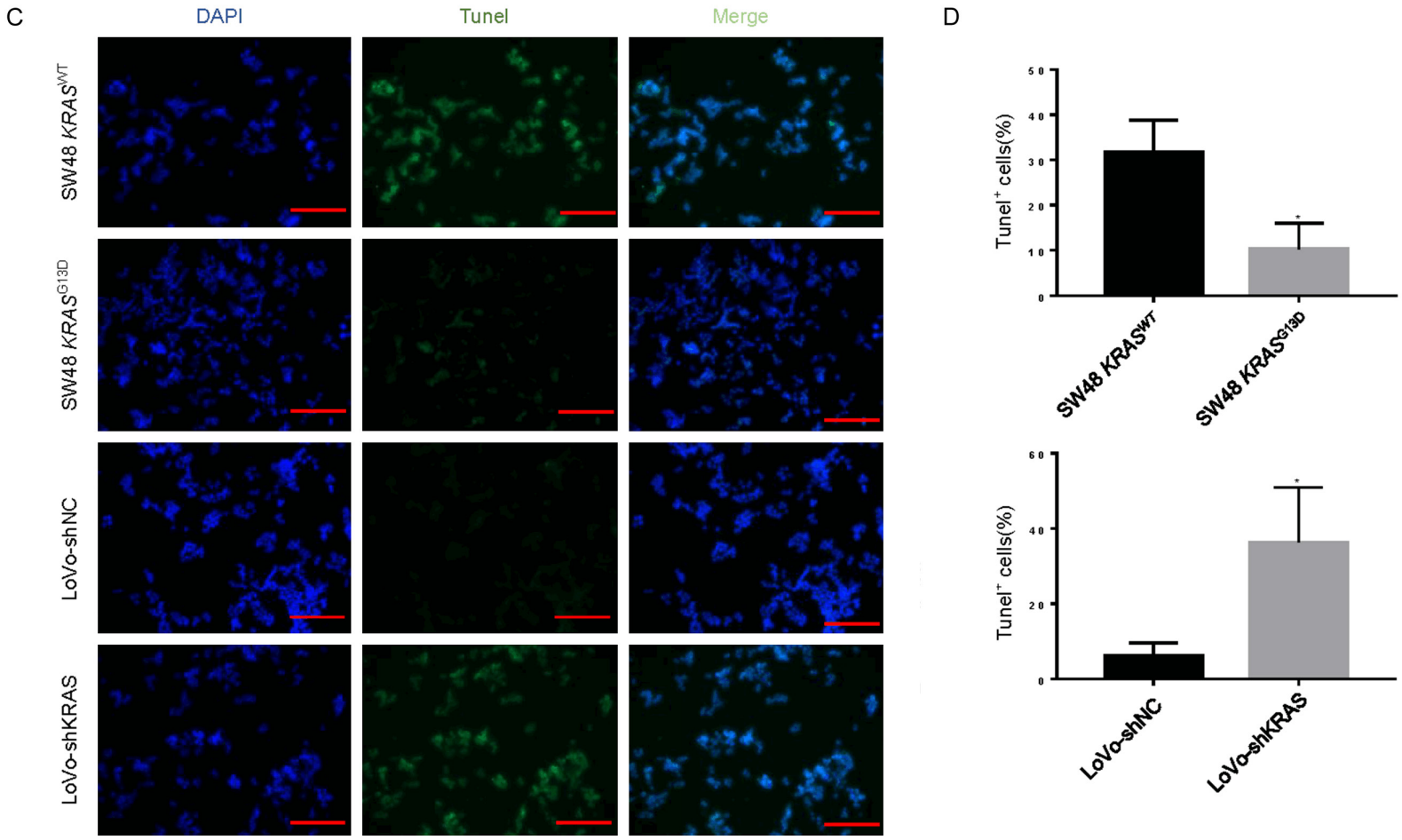

Figure 3. Chiauranib selectively promotes *KRAS* wild-type CRC cells apoptosis. A. Flow cytometric analysis of apoptosis in the indicated cells after treatment with 0, 2, 4, 8 μM Chiauranib for 48 hours. B. Statistical analysis of apoptotic cells detected by flow cytometry. Bars represent the mean ± SD of three independent experiments; $*P < 0.05$, $**P < 0.01$ and $***P < 0.001$ was compared with 0 μM Chiauranib. C. Representative images of TUNEL staining in the indicated $KRAS^{WT}$ SW48, $KRAS^{G13D}$ SW48, LoVo-shNC and LoVo-shKRAS cells after treatment with 4 μM Chiauranib for 48 hours. Scale bar, 50 μm. D. Statistical analysis of TUNEL staining. Bars represented the mean ± SD of three independent experiments; $*P < 0.05$ was compared with $KRAS^{WT}$ SW48 group or LoVo-shNC group.

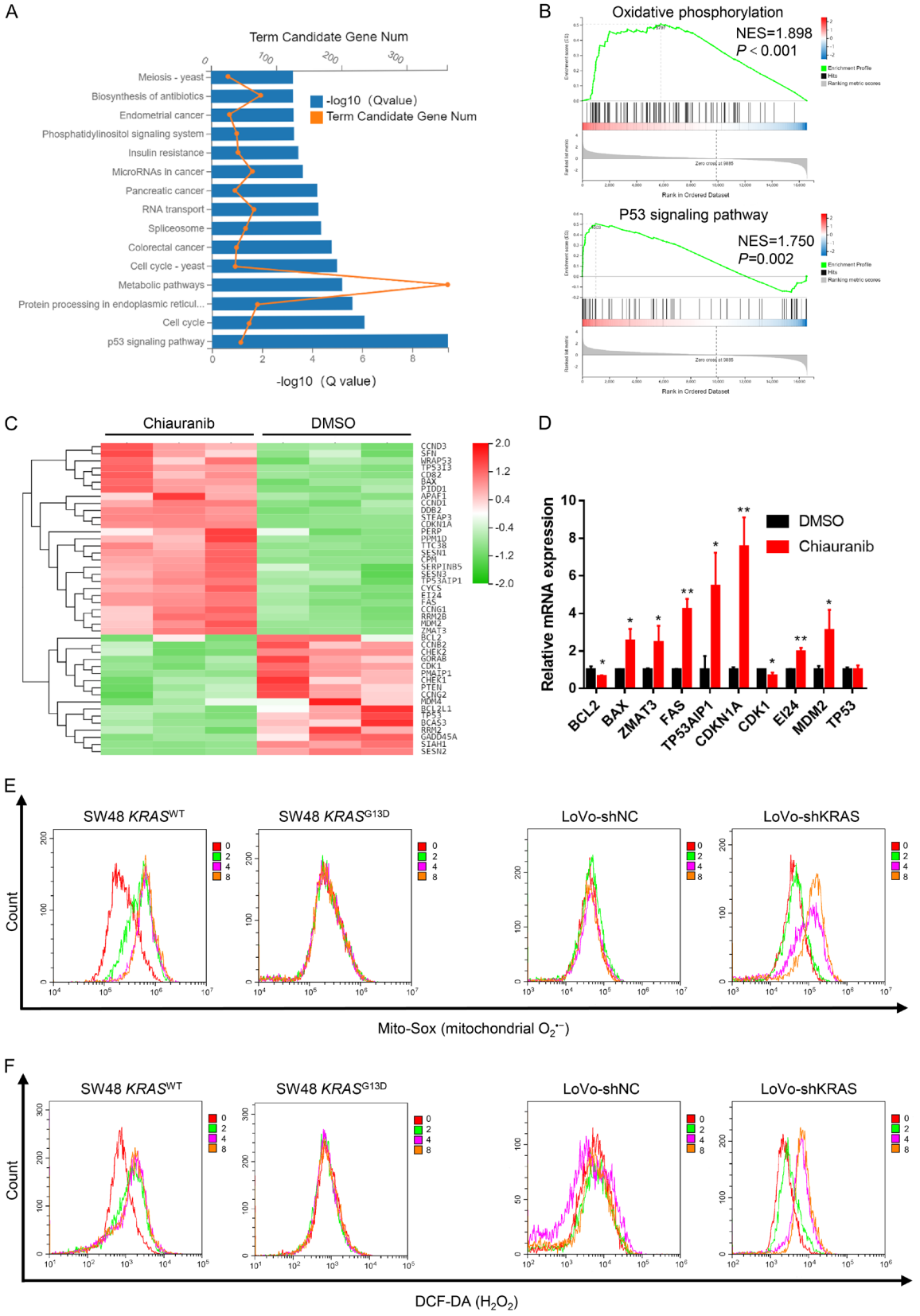

Figure 4. Chiauranib alters gene sets related to ROS in *KRAS* wild-type CRC cells. (A) KEGG pathway enrichment between DMSO and Chiauranib groups, based on RNA-Seq analysis. (B) Gene set enrichment analysis (GSEA) analysis

showed that DEGs were positively correlated with oxidative phosphorylation and the p53 signaling pathway. (C) Heat map of 44 DEGs related to oxidative phosphorylation and the p53 signaling pathway. (D) Q-PCR of genes related to the p53 signaling pathway of SW48 cells after treatment with 4 μM Chiauranib for 48 hours. (E, F) *KRAS*^{WT} SW48, *KRAS*^{G13D} SW48, LoVo-shNC and LoVo-shKRAS cells were incubated for 30 min in the presence of Mito-SOX or DCH-DA. Representative flow cytometry plots showed the separate analysis of (E) mitochondrial $O_2^{\bullet-}$ and (F) H_2O_2 in SW48 cells after treatment with 4 μM Chiauranib for 48 hours.

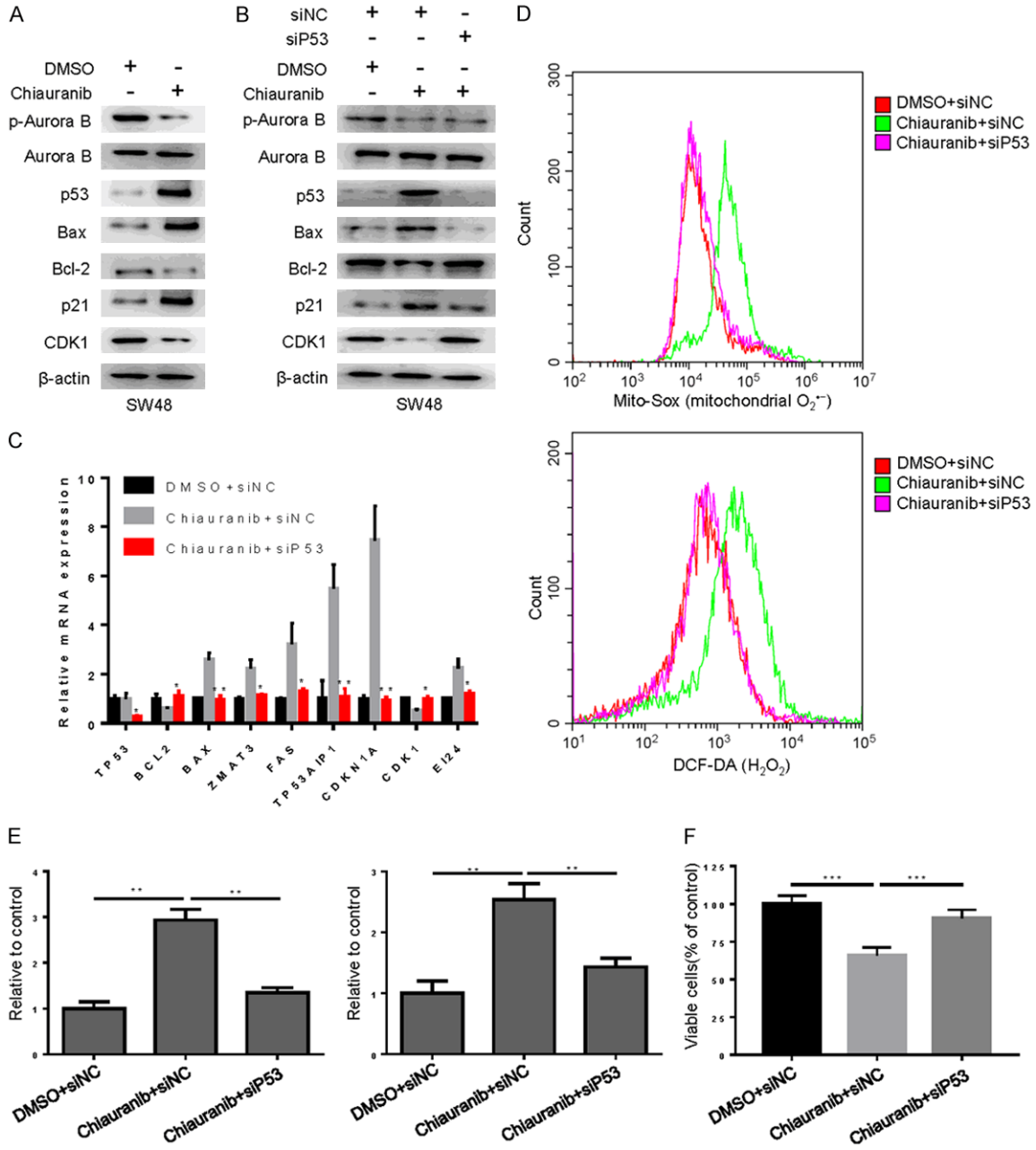

Figure 5. Chiauranib induces ROS of *KRAS* wild-type CRC cells by activating the p53 signaling pathway. (A) Western blot of proteins related to the p53 signaling pathway in SW48 cells after treatment with 4 μM Chiauranib for 48 hours. (B, C) SW48 cells were infected with siRNA to knock down p53 and treatment with 4 μM Chiauranib for 48 hours, followed by (B) Western blot and (C) Q-PCR analysis. (D) Representative flow cytometry plots showed the separate analysis of mitochondrial $O_2^{\bullet-}$ and H_2O_2 in SW48 cells after infected with siRNA to knock down p53, and treatment with 4 μM Chiauranib for 48 hours. (E) Statistical analysis of mitochondrial $O_2^{\bullet-}$ and H_2O_2. Bars represent the mean ± SD of three independent experiments; $^*P < 0.05$, $^{**}P < 0.01$ and $^{***}P < 0.001$. (F) Cell viability detection in SW48 cells after infected with siRNA to knock down p53, and treatment with 4 μM Chiauranib for 48 hours.

tion of the p53 signaling pathway. The increased ROS levels induced by Chiauranib were dramatically abrogated by knockdown of p53 (**Figure 5D**, **5E**). Moreover, silencing p53 substantially increased the cell viability reduction by Chiauranib treatment in *KRAS* wild-type CRC cells (**Figure 5F**). These data collectively suggested that Chiauranib induced intracellular ROS levels via activating the p53 signaling pathway in *KRAS* wild-type CRC cells.

KRAS mutation CRC cells are resistant to ROS induced by Chiauranib via upregulating Nrf2

Although we found the role and mechanism of ROS production induced by Chiauranib in *KRAS* wild-type CRC cells, the mechanism of Chiauranib resistance in *KRAS* mutation cells were not precise. Impressively, Chiauranib treatment inhibited phosphorylation of Aurora B in LoVo-shNC cells, but p53 was not affected. However, both of Aurora B phosphorylation and p53 expression could be inhibited in LoVo-shKRAS cells (**Figure 6A**). Recently, several studies have suggested that KRAS maintained low p53 levels by activating Nrf2 expression [22]. Meanwhile, western blot results revealed that Nrf2 was downregulated and p53 was upregulated in *KRAS*-silenced LoVo cells, and reverse changes in *KRAS* mutation LoVo cells (**Figure 6B**). Therefore, we hypothesized that *KRAS* mutation promoted the expression of Nrf2 and thus inhibited the increase of the p53 signaling pathway, making *KRAS* mutation cells resistant to Chiauranib.

To test this hypothesis, we further detected the p53 signaling pathway and cell viability in Nrf2 knockdown cell after treatment with Chiauranib. Interestingly, our results suggested that silencing Nrf2 activated the p53 signaling pathway and inhibited cell viability in *KRAS* mutation LoVo cells with Chiauranib treatment (**Figure 6C-E**). Moreover, silencing Nrf2 promoted ROS production in LoVo cells with Chiauranib treatment (**Figure 6F**, **6G**). Above all, *KRAS* mutation CRC cells were resistant to ROS induced by Chiauranib through upregulating Nrf2.

Chiauranib selectively inhibits the growth of KRAS wild-type CRC cells in vivo

To further verify whether pharmacological Chiauranib was sufficient to mediate anti-tumor effects in a preclinical model, we generated mouse Xenograft Models by subcutaneous injection of SW48 and LoVo cells. One week after injection, tumor-bearing mice were randomized into two groups and administered intragastrically with vehicle or Chiauranib (40 mg/kg) once every three days. While treatment with Chiauranib in LoVo bearing Xenograft Models had little anti-tumor effects than the vehicle control, Chiauranib treatment significantly inhibited SW48 bearing Xenograft Models tumor growth (**Figure 7A-C**; Supplementary Figure 4). No remarkable weight loss or signs of morbidity were observed in the mouse Xenograft Models treated with Chiauranib during the experiment (Supplementary Figure 5). Moreover, Ki67 staining and TUNEL staining of the SW48 Xenograft Models tumors showed that Chiauranib inhibited *KRAS* wild-type CRC cells proliferation and induced apoptosis (**Figure 7D-G**). Noticeably, DHE staining samples showed Chiauranib increased accumulation of superoxide anion radicals in SW48 Xenograft Models tumors consistent with *in vitro* experimental results (**Figure 7H**, **7I**). Our findings provided direct evidence of the safety and efficacy of Chiauranib for *KRAS* wild-type CRC treatment in preclinical models (**Figure 8**).

Discussion

Abnormal KRAS signaling played a crucial role in tumor growth and was usually associated with resistance to anti-EGFR therapy. Our recent research found that metformin selectively inhibited metastatic *KRAS* mutation CRC by decreasing excretion through silencing channel protein MATE1 [18]. On the other hand, 50% of *KRAS* wild-type CRC patients failed to respond to the anti-EGFR antibody cetuximab treatment, which has been proven effective in the treatment of *KRAS* wild-type CRC patients [7]. Therefore, it is imperative to find new drugs targeting *KRAS* wild-type CRC. Recently, the anti-tumor activity of Chiauranib has been explored in various cancers, including Non-Hodgkin's lymphomas, acute myeloid leukemia, hepatocellular carcinoma, and gastric cancer [9, 10]. Surprisingly, in our experiments, we found for the first time that Chiauranib selectively inhibited the growth of *KRAS* wild-type CRC cells. This dramatic effect was further confirmed in mouse

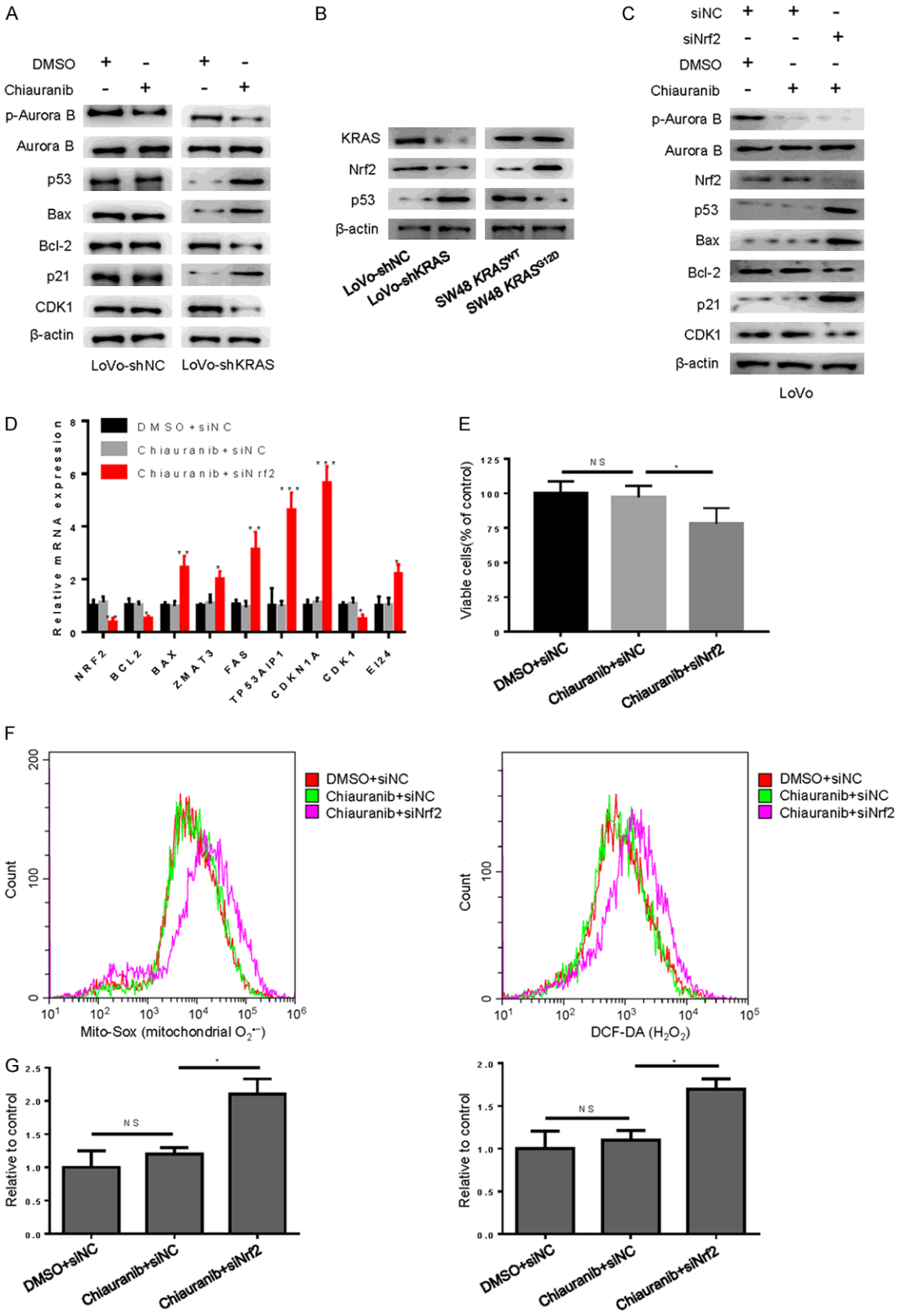
A
DMSO
Chiauranib
p-Aurora B
Aurora B
p53
Bax
Bcl-2
p21
CDK1
β-actin
LoVo-shNC
LoVo-shKRAS
B
KRAS
Nrf2
p53
β-actin
LoVo-shNC
LoVo-shKRAS
SW48 KRASWT
SW48 KRASG12D
C
siNC
siNrf2
DMSO
Chiauranib
p-Aurora B
Aurora B
Nrf2
p53
Bax
Bcl-2
p21
CDK1
β-actin
LoVo
D
DMSO+siNC
Chiauranib+siNC
Chiauranib+siNrf2
Relative mRNA expression
NRF2
BCL2
BAX
ZMAT3
FAS
TP53AIP1
CDKN1A
CDK1
EI24
E
Viable cells(% of control)
NS
DMSO+siNC
Chiauranib+siNC
Chiauranib+siNrf2
F
Count
Mito-Sox (mitochondrial O2•−)
DCF-DA (H2O2)
DMSO+siNC
Chiauranib+siNC
Chiauranib+siNrf2
G
Relative to control
NS
DMSO+siNC
Chiauranib+siNC
Chiauranib+siNrf2

Figure 6. *KRAS* mutation CRC cells are resistant to ROS induced by Chiauranib via upregulating Nrf2. (A) Western blot of proteins related to the p53 signaling pathway in LoVo-shNC and LoVo-shKRAS cells after treatment with 4 μM Chiauranib for 48 hours. (B) Western blot of Nrf2 in the indicated cells. (C-E) LoVo cells were infected with siRNA to knock down Nrf2, followed by (C) Western blot and (D) Q-PCR analysis and (E) cell viability detection. (F) Representative flow cytometry plots show the separate analysis of mitochondrial $O_2^{\bullet-}$ and H_2O_2 in LoVo cells after infected with siRNA to knock down Nrf2, and treatment with 4 μM Chiauranib for 48 hours. (G) Statistical analysis of mitochondrial $O_2^{\bullet-}$ and H_2O_2. Bars represented the mean ± SD of three independent experiments; $*P < 0.05$, $**P < 0.01$ and $***P < 0.001$.

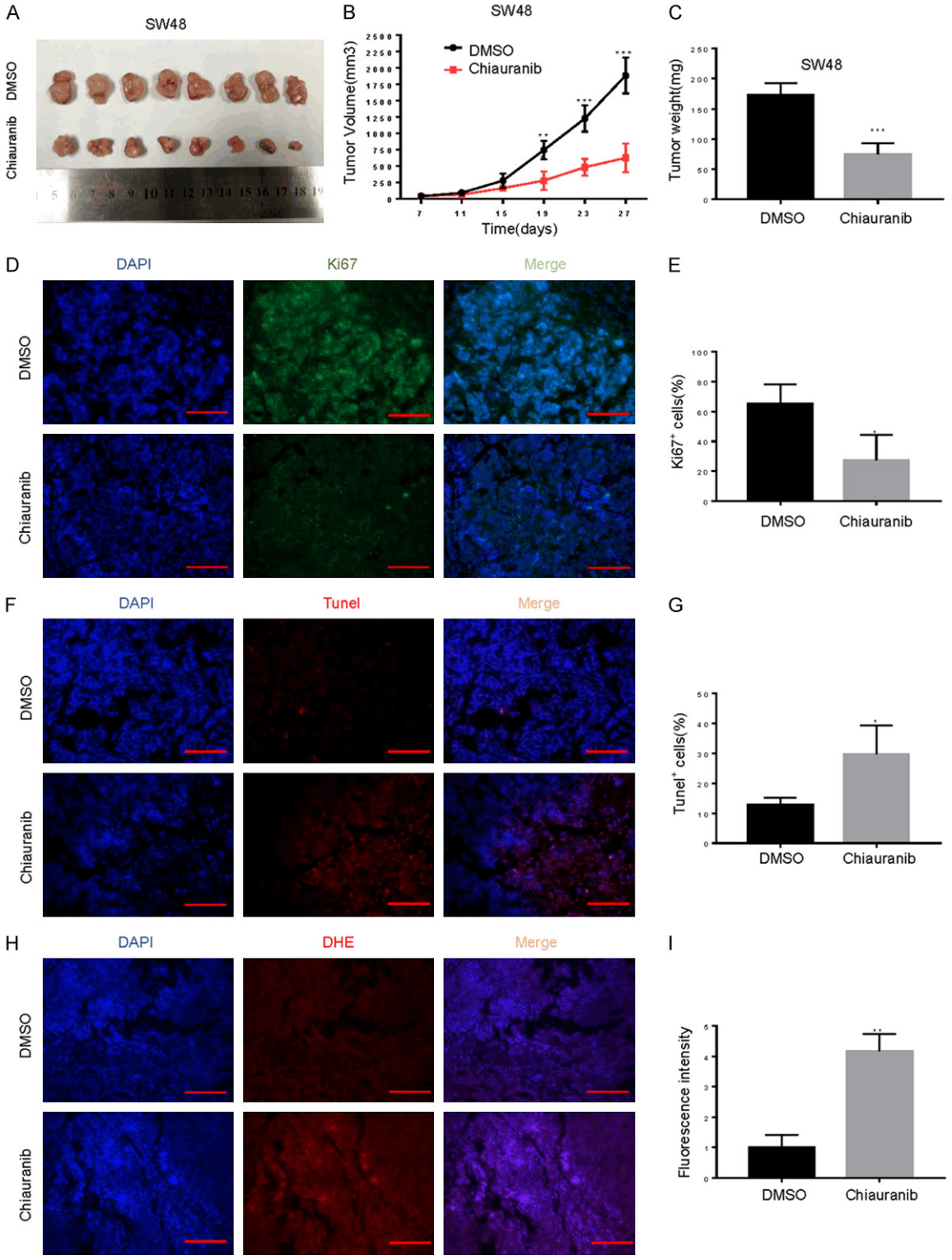

Figure 7. Chiauranib selectively inhibits the growth of *KRAS* wild-type CRC cells *in vivo*. (A-C) (A) The representative morphology, (B) tumor growth rate, and (C) tumor weight were shown as a result of treatment with Chiauranib (40 mg/kg) once every three days in SW48 Xenograft Models. Data are shown as mean ± SD; $^{**}P < 0.01$, $^{***}P < 0.001$. (D) Representative images of Ki67 staining in Xenograft Models tumors. Scale bar, 50 μm. (E) Statistical analysis of Ki67 staining. (F) Representative images of TUNEL staining in Xenograft Models tumors. Scale bar, 50 μm. (G) Statistical analysis of TUNEL staining. (H) Representative images of DHE staining in Xenograft Models tumors. Scale bar, 50 μm. (I) Statistical analysis of DHE staining. Data were expressed as mean ± SD; $^{*}P < 0.05$, $^{**}P < 0.01$.

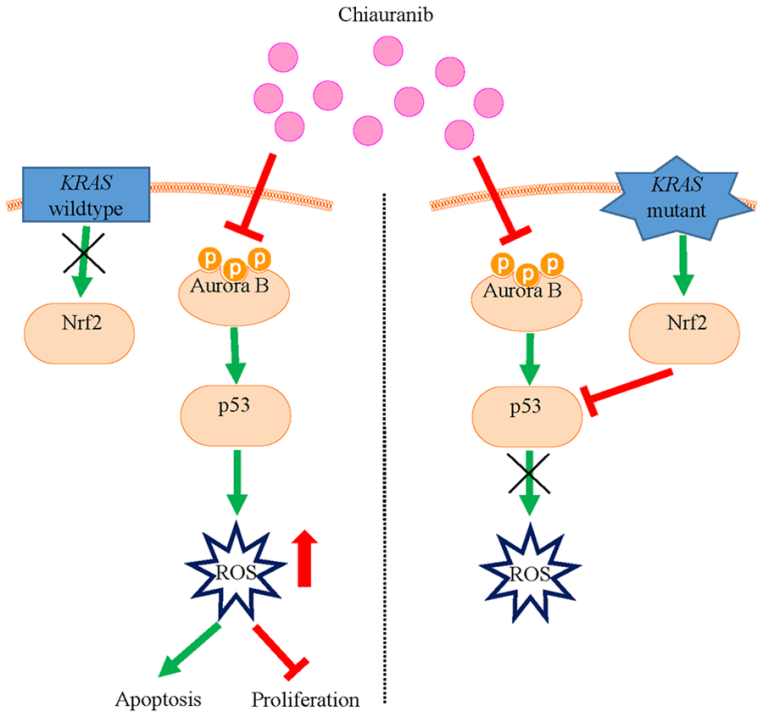

Figure 8. Simplified model depicting the pathway through how Chiauranib regulates *KRAS* wild-type CRC growth.

Xenograft Models. Our study has put forward the possibility of a therapeutic strategy for *KRAS* wild-type CRC patients by using Chiauranib.

Given the complex landscape of genetic alterations in cancer, it does not mean that chemotherapy drugs are useful for every patient. In our initial experiment, we tested the effect of Chiauranib on four CRC cell lines (LoVo, HCT116, SW48, $CaCO_2$). Surprisingly, only SW48 and $CaCO_2$ cells were sensitive to Chiauranib, while LoVo and HCT116 cells were resistant to Chiauranib (**Figure 1**). After carefully searching, we found that only the *KRAS* gene mutated in LoVo cells among the common CRC mutation genes of *KRAS*, *BRAF*, *PIK3CA*, *PTEN*, and *TP53* [20]. *KRAS* mutation also occurred in HCT116 cells, whereas both of SW48 and $CaCO_2$ cells were *KRAS* wild-type cells. Further experiments showed that Chiauranib selectively inhibited proliferation and induced apoptosis of *KRAS* wild-type CRC cells (**Figures 2**, **3**). Previous studies on various types of tumors have not found that some tumor cells are resistant to Chiauranib, possibly because *KRAS* gene mutation was not common in these tumors. However, the rate of *KRAS* mutation in CRC patients was as high as 30-50% [23]. It is possible that Chiauranib resistance may also exist in other types of tumors with frequent *KRAS* mutations, such as lung cancer and pancreatic cancer, which is worthy of further exploration.

To further explore the molecular mechanisms of Chiauranib inhibiting *KRAS* wild-type CRC, we determined the overall gene expression pattern of SW48 cells treated with Chiauranib by RNA sequence analysis (Supplementary Figure 1). Through KEGG and GSEA analysis, we found that the p53 signaling pathway and oxidative phosphorylation pathway were most significantly regulated, respectively (**Figure 4A**, **4B**; Supplementary Figure 2). P53 signaling pathway played an essential role in DNA damage response, cell cycle, and apoptosis [15]. ROS was a direct representation of the activation of oxidative phosphorylation pathway, which could be modulated by the p53 signaling pathway [24, 25]. Activation of the p53 signaling pathway led to the accumulation of ROS, thus inhibiting cell proliferation and inducing apoptosis [25].

Some studies also suggested that ROS could regulate the p53 signaling pathway, indicating that ROS and p53 signaling pathways have positive feedback [26]. In our research, we found that the p53 signaling pathway and ROS related molecules were significantly changed after Chiauranib treatment, but the mRNA level of p53 did not change (**Figure 4C**, **4D**). These results indicated that Chiauranib activated ROS through direct stimulation of p53 signaling pathway via p53 post-transcriptional regulation. Aurora B was a member of the chromosomal passenger complex, which a key regulator of mitosis and cell cycle [27]. Several lines of evidence suggested that Aurora B was prominently overexpressed in CRC and positively correlated with advanced tumor stages [28-30]. In addition, Aurora B has been shown to block the anti-tumor function of p53 through promoting its degradation, and otherwise, promote malignant transformation via activating RAS signaling [31, 32]. While whether the novel serine-threonine-kinases-targeted agent Chiauranib can be considered as an alternative choice at all times should be illustrated. In this study, our results demonstrated that Chiauranib inhibited Aurora B phosphorylation, resulting in an increased in p53 expression, thus inducing ROS production in *KRAS* wild-type CRC cells (**Figure 5**). Notably, *p53* mutation also occurs frequently in many types of tumors, including CRC [33]. Whether *p53* mutation could also lead to resistance to Chiauranib needs further study. However, as we known, Chiauranib is a multi-target small molecule inhibitor, which was very likely to play an anti-tumor role through other pathways in *p53* mutant cells.

Nrf2 pathway was closely related to antioxidation, lowering intracellular ROS levels, and reducing intracellular environment [34]. The increase of Nrf2 expression induced by *KRAS* was a new mechanism of Nrf2 antioxidant program activation, which can steadily improve Nrf2 antioxidant basic program by increasing Nrf2 transcription [22, 35]. *KRAS*-directed increased expression of Nrf2 was evident in tissues of *KRAS* mutation CRC patients consistent with our *in vitro* results (**Figure 6B**). Moreover, genetic targeting of the Nrf2 pathway impaired $KRAS^{G12D}$-induced tumorigenesis and development *in vivo* [36, 37]. Therefore, Nrf2 antioxidant and cellular detoxification programs were crucial mediators of Chiauranib resistance in *KRAS* mutation CRC.

Impressively, the results of our animal experiments showed that Chiauranib has significant efficacy and safety, consistent with the phase I clinical trial (NCT03074825) (**Figure 7**). During the investigation, no significant weight loss or signs of disease were observed in the xenograft model treated with Chiauranib (Supplementary Figure 5). However, the commonly used chemotherapy drugs such as oxaliplatin and irinotecan have apparent side effects [38, 39]. Chiauranib may replace these chemotherapeutic drugs and become the new choice for the treatment of *KRAS* wild-type CRC. Notably, we found that Chiauranib slightly inhibited tumor growth on day 27, but it was not observed at any previous point (Supplementary Figure 4). This result suggested that long-term Chiauranib treatment may also inhibit *KRAS* mutation CRC growth *in vivo*, which needed to be confirmed by observation for a longer time. Recent findings provided evidence that Chiauranib could not only directly cause tumor cell death, but also restore anti-tumor immunity by altering some crucial components of the tumor microenvironment, which might build up the foundation for combined immunotherapies [40]. Therefore, it is worthy to obtain more convincing data to see whether Chiauranib can be therapeutically employed in *KRAS* mutation CRC treatment by regulating tumor microenvironment.

In conclusion, precision medicine is an emerging method that guides patients to receive more effective treatment strategies according to individual differences. We reveal that Chiauranib induces p53 upregulation, resulting in ROS accumulation, thus inhibiting cell proliferation and inducing apoptosis. This study suggests that *KRAS* wild-type status could be a potential biomarker for using Chiauranib in CRC patients. Further clinical trials are necessary to verify efficacy and safety from Chiauranib treatment in CRC patients.

Acknowledgements

This study was supported by the fund from Guangzhou Institute of Pediatrics/Guangzhou Women and Children's Medical Center (YIP-2019-021). National Nature Science Found-

ation of China (81902693); the Natural Science Foundation of Guangdong Province (2018A030310298); Educational Commission of Guangdong Province (2017KTSCX155); Guangdong Basic and Applied Basic Research Foundation (NO 2019A1515011318); Shenzhen Science and Technology Innovation Commission Basic Research Foundation (NO JCYJ20180307150637015). All animal experimental protocols were approved by the Institutional Animal Care and Use Committee of Sun Yat-sen University (Guangdong Province, China).

Disclosure of conflict of interest

None.

Address correspondence to: Honghai Hong, Department of Clinical Laboratory, The Third Affiliated Hospital of Guangzhou Medical University, Guangzhou, Guangdong, China. Tel: +86-020-87330634; E-mail: gaolaosao@126.com; Caiqi Ma, Reproductive Medical Center, Guangzhou Women and Children's Medical Center of Sun Yat-sen University, Guangzhou, Guangdong, China. Tel: +86-020-87330634; E-mail: phelix-ma@foxmail.com; Zhaofan Luo, Department of Clinical Laboratory, The Seventh Affiliated Hospital of Sun Yat-sen University, Shenzhen, Guangdong, China. Tel: +86-0759-81206592; E-mail: luozhaofan@qq.com

References

[1] Siegel RL, Miller KD and Jemal A. Cancer statistics, 2018. CA Cancer J Clin 2018; 68: 7-30.

[2] Tan KK, Lopes Gde L Jr and Sim R. How uncommon are isolated lung metastases in colorectal cancer? A review from database of 754 patients over 4 years. J Gastrointest Surg 2009; 13: 642-648.

[3] Cremolini C, Loupakis F, Antoniotti C, Lupi C, Sensi E, Lonardi S, Mezi S, Tomasello G, Ronzoni M, Zaniboni A, Tonini G, Carlomagno C, Allegrini G, Chiara S, D'Amico M, Granetto C, Cazzaniga M, Boni L, Fontanini G and Falcone A. FOLFOXIRI plus bevacizumab versus FOLFIRI plus bevacizumab as first-line treatment of patients with metastatic colorectal cancer: updated overall survival and molecular subgroup analyses of the open-label, phase 3 TRIBE study. Lancet Oncol 2015; 16: 1306-1315.

[4] Yaeger R, Chatila WK, Lipsyc MD, Hechtman JF, Cercek A, Sanchez-Vega F, Jayakumaran G, Middha S, Zehir A, Donoghue MTA, You D, Viale A, Kemeny N, Segal NH, Stadler ZK, Varghese AM, Kundra R, Gao J, Syed A, Hyman DM, Vakiani E, Rosen N, Taylor BS, Ladanyi M, Berger MF, Solit DB, Shia J, Saltz L and Schultz N. Clinical sequencing defines the genomic landscape of metastatic colorectal cancer. Cancer Cell 2018; 33: 125-136, e123.

[5] Allegra CJ, Rumble RB, Hamilton SR, Mangu PB, Roach N, Hantel A and Schilsky RL. Extended RAS gene mutation testing in metastatic colorectal carcinoma to predict response to anti-epidermal growth factor receptor monoclonal antibody therapy: american society of clinical oncology provisional clinical opinion update 2015. J Clin Oncol 2016; 34: 179-185.

[6] Douillard JY, Oliner KS, Siena S, Tabernero J, Burkes R, Barugel M, Humblet Y, Bodoky G, Cunningham D, Jassem J, Rivera F, Kocakova I, Ruff P, Blasinska-Morawiec M, Smakal M, Canon JL, Rother M, Williams R, Rong A, Wiezorek J, Sidhu R and Patterson SD. Panitumumab-FOLFOX4 treatment and RAS mutations in colorectal cancer. N Engl J Med 2013; 369: 1023-1034.

[7] Laurent-Puig P, Cayre A, Manceau G, Buc E, Bachet JB, Lecomte T, Rougier P, Lievre A, Landi B, Boige V, Ducreux M, Ychou M, Bibeau F, Bouche O, Reid J, Stone S and Penault-Llorca F. Analysis of PTEN, BRAF, and EGFR status in determining benefit from cetuximab therapy in wild-type KRAS metastatic colon cancer. J Clin Oncol 2009; 27: 5924-5930.

[8] Zhou Y, Shan S, Li ZB, Xin LJ, Pan DS, Yang QJ, Liu YP, Yue XP, Liu XR, Gao JZ, Zhang JW, Ning ZQ and Lu XP. CS2164, a novel multi-target inhibitor against tumor angiogenesis, mitosis and chronic inflammation with anti-tumor potency. Cancer Sci 2017; 108: 469-477.

[9] Deng M, Zhao H, Chen Q, Zhao J, Shi Y, Yu L, Fang Z and Xu B. CS2164 suppresses acute myeloid leukemia cell growth via inhibiting VEGFR2 signaling in preclinical models. Eur J Pharmacol 2019; 853: 193-200.

[10] Deng M, Shi Y, Chen K, Zhao H, Wang Y, Xie S, Zhao J, Luo Y, Fang Z, Fan Y and Xu B. CS2164 exerts an antitumor effect against human Non-Hodgkin's lymphomas in vitro and in vivo. Exp Cell Res 2018; 369: 356-362.

[11] Sun Y, Yang L, Hao X, Liu Y, Zhang J, Ning Z and Shi Y. Phase I dose-escalation study of chiauranib, a novel angiogenic, mitotic, and chronic inflammation inhibitor, in patients with advanced solid tumors. J Hematol Oncol 2019; 12: 9.

[12] Zhou J, Zhang L, Wang M, Zhou L, Feng X, Yu L, Lan J, Gao W, Zhang C, Bu Y, Huang C, Zhang H and Lei Y. CPX targeting DJ-1 triggers ROS-induced cell death and protective autophagy in colorectal cancer. Theranostics 2019; 9: 5577-5594.

[13] Chang TC, Wei PL, Makondi PT, Chen WT, Huang CY and Chang YJ. Bromelain inhibits the ability of colorectal cancer cells to proliferate via activation of ROS production and autophagy. PLoS One 2019; 14: e0210274.
[14] Ju HQ, Lu YX, Chen DL, Zuo ZX, Liu ZX, Wu QN, Mo HY, Wang ZX, Wang DS, Pu HY, Zeng ZL, Li B, Xie D, Huang P, Hung MC, Chiao PJ and Xu RH. Modulation of redox homeostasis by inhibition of MTHFD2 in colorectal cancer: mechanisms and therapeutic implications. J Natl Cancer Inst 2019; 111: 584-596.
[15] Neitzel C, Seiwert N, Goder A, Diehl E, Weber C, Nagel G, Stroh S, Rasenberger B, Christmann M and Fahrer J. Lipoic acid synergizes with antineoplastic drugs in colorectal cancer by targeting p53 for proteasomal degradation. Cells 2019; 8: 794.
[16] Meek DW. Regulation of the p53 response and its relationship to cancer. Biochem J 2015; 469: 325-346.
[17] Wu L, Ma CA, Zhao Y and Jain A. Aurora B interacts with NIR-p53, leading to p53 phosphorylation in its DNA-binding domain and subsequent functional suppression. J Biol Chem 2011; 286: 2236-2244.
[18] Xie J, Xia L, Xiang W, He W, Yin H, Wang F, Gao T, Qi W, Yang Z, Yang X, Zhou T and Gao G. Metformin selectively inhibits metastatic colorectal cancer with the KRAS mutation by intracellular accumulation through silencing MATE1. Proc Natl Acad Sci U S A 2020; 117: 13012-13022.
[19] Jiang P, Huang M, Qi W, Wang F, Yang T, Gao T, Luo C, Deng J, Yang Z, Zhou T, Zou Y, Gao G and Yang X. FUBP1 promotes neuroblastoma proliferation via enhancing glycolysis-a new possible marker of malignancy for neuroblastoma. J Exp Clin Cancer Res 2019; 38: 400.
[20] Ahmed D, Eide PW, Eilertsen IA, Danielsen SA, Eknaes M, Hektoen M, Lind GE and Lothe RA. Epigenetic and genetic features of 24 colon cancer cell lines. Oncogenesis 2013; 2: e71.
[21] Saini H, Hakeem I, Mukherjee S, Chowdhury S and Chowdhury R. Autophagy regulated by gain of function mutant p53 enhances proteasomal inhibitor-mediated cell death through induction of ROS and ERK in lung cancer cells. J Oncol 2019; 2019: 6164807.
[22] Zhang Y, Song J, Zhao Z, Yang M, Chen M, Liu C, Ji J and Zhu D. Single-cell transcriptome analysis reveals tumor immune microenvironment heterogenicity and granulocytes enrichment in colorectal cancer liver metastases. Cancer Lett 2020; 470: 84-94.
[23] Vogelstein B, Fearon ER, Hamilton SR, Kern SE, Preisinger AC, Leppert M, Nakamura Y, White R, Smits AM and Bos JL. Genetic alterations during colorectal-tumor development. N Engl J Med 1988; 319: 525-532.
[24] Kutuk O, Aytan N, Karakas B, Kurt AG, Acikbas U, Temel SG and Basaga H. Biphasic ROS production, p53 and BIK dictate the mode of cell death in response to DNA damage in colon cancer cells. PLoS One 2017; 12: e0182809.
[25] Chen P, Luo X, Nie P, Wu B, Xu W, Shi X, Chang H, Li B, Yu X and Zou Z. CQ synergistically sensitizes human colorectal cancer cells to SN-38/CPT-11 through lysosomal and mitochondrial apoptotic pathway via p53-ROS crosstalk. Free Radic Biol Med 2017; 104: 280-297.
[26] Srinivas US, Tan BWQ, Vellayappan BA and Jeyasekharan AD. ROS and the DNA damage response in cancer. Redox Biol 2019; 25: 101084.
[27] Zhao Z, Jin G, Yao K, Liu K, Liu F, Chen H, Wang K, Gorja DR, Reddy K, Bode AM, Guo Z and Dong Z. Aurora B kinase as a novel molecular target for inhibition the growth of osteosarcoma. Mol Carcinog 2019; 58: 1056-1067.
[28] Siegel RL, Miller KD, Fedewa SA, Ahnen DJ, Meester RGS, Barzi A and Jemal A. Colorectal cancer statistics, 2017. CA Cancer J Clin 2017; 67: 177-193.
[29] Pohl A, Azuma M, Zhang W, Yang D, Ning Y, Winder T, Danenberg K and Lenz HJ. Pharmacogenetic profiling of Aurora kinase B is associated with overall survival in metastatic colorectal cancer. Pharmacogenomics J 2011; 11: 93-99.
[30] Sijare F, Geissler AL, Fichter CD, Hergeth SP, Bogatyreva L, Hauschke D, Schneider R, Werner M and Lassmann S. Aurora B expression and histone variant H1.4S27 phosphorylation are no longer coordinated during metaphase in aneuploid colorectal carcinomas. Virchows Arch 2015; 466: 503-515.
[31] Kanda A, Kawai H, Suto S, Kitajima S, Sato S, Takata T and Tatsuka M. Aurora-B/AIM-1 kinase activity is involved in Ras-mediated cell transformation. Oncogene 2005; 24: 7266-7272.
[32] Kosik A, Bekier ME, Katusin JD, Kaur H, Zhou X, Diakonova M, Chadee DN and Taylor WR. Investigating the role of Aurora kinases in RAS signaling. J Cell Biochem 2009; 106: 33-41.
[33] Bond CE, Umapathy A, Ramsnes I, Greco SA, Zhen Zhao Z, Mallitt KA, Buttenshaw RL, Montgomery GW, Leggett BA and Whitehall VL. p53 mutation is common in microsatellite stable, BRAF mutant colorectal cancers. Int J Cancer 2012; 130: 1567-1576.
[34] DeNicola GM, Karreth FA, Humpton TJ, Gopinathan A, Wei C, Frese K, Mangal D, Yu KH, Yeo CJ, Calhoun ES, Scrimieri F, Winter JM, Hruban RH, Iacobuzio-Donahue C, Kern SE, Blair IA and Tuveson DA. Oncogene-induced

Nrf2 transcription promotes ROS detoxification and tumorigenesis. Nature 2011; 475: 106-109.

[35] Ferino A, Rapozzi V and Xodo LE. The ROS-KRAS-Nrf2 axis in the control of the redox homeostasis and the intersection with survival-apoptosis pathways: implications for photodynamic therapy. J Photochem Photobiol B 2020; 202: 111672.

[36] Satoh H, Moriguchi T, Takai J, Ebina M and Yamamoto M. Nrf2 prevents initiation but accelerates progression through the Kras signaling pathway during lung carcinogenesis. Cancer Res 2013; 73: 4158-4168.

[37] Galan-Cobo A, Sitthideatphaiboon P, Qu X, Poteete A, Pisegna MA, Tong P, Chen PH, Boroughs LK, Rodriguez MLM, Zhang W, Parlati F, Wang J, Gandhi V, Skoulidis F, DeBerardinis RJ, Minna JD and Heymach JV. LKB1 and KEAP1/NRF2 pathways cooperatively promote metabolic reprogramming with enhanced glutamine dependence in KRAS-mutant lung adenocarcinoma. Cancer Res 2019; 79: 3251-3267.

[38] Drott J, Fomichov V, Starkhammar H, Borjeson S, Kjellgren K and Bertero C. Oxaliplatin-induced neurotoxic side effects and their impact on daily activities: a longitudinal study among patients with colorectal cancer. Cancer Nurs 2019; 42: E40-E48.

[39] Xu Y, Li Q, Ma HY, Sun T, Xiang RL and Di F. Therapeutic effect and side effects of bevacizumab combined with Irinotecan in the treatment of paediatric intracranial tumours: meta-analysis and systematic review. J Clin Pharm Ther 2020; [Epub ahead of print].

[40] Zhou Y, Fu C, Kong Y, Pan D, Wang Y, Huang S, Li Z, Ning Z, Lu X, Shan S and Xin L. Antitumor and immunomodulatory effects of a novel multitarget inhibitor, CS2164, in mouse hepatocellular carcinoma models. Anticancer Drugs 2019; 30: 909-916.

Supplementary Table 1. Primer sequence

Primer	Sequence (5' to 3')
BCL2-F	GGTGGGGTCATGTGTGTGG
BCL2-R	CGGTTCAGGTACTCAGTCATCC
BAX-F	CCCGAGAGGTCTTTTTCCGAG
BAX-R	CCAGCCCATGATGGTTCTGAT
ZMAT3-F	AGAAGCCTTTTGGGCAGGAG
ZMAT3-R	TGCTGCATAGTAATTTCGGAGTT
FAS-F	TCTGGTTCTTACGTCTGTTGC
FAS-R	CTGTGCAGTCCCTAGCTTTCC
TP53AIP1-F	GGTGCCCAAGTTCACGGAG
TP53AIP1-R	CTGGAGAGACCTAGACCAAGG
CDKN1A-F	TGTCCGTCAGAACCCATGC
CDKN1A-R	AAAGTCGAAGTTCCATCGCTC
CDK1-F	AAACTACAGGTCAAGTGGTAGCC
CDK1-R	TCCTGCATAAGCACATCCTGA
EI24-F	TGCCAGAGGAATCAAAGACTCC
EI24-R	TCTCTTGCTTCCGCTCTATACT
MDM2-F	GAATCATCGGACTCAGGTACATC
MDM2-R	TCTGTCTCACTAATTGCTCTCCT
TP53-F	CAGCACATGACGGAGGTTGT
TP53-R	TCATCCAAATACTCCACACGC
β-actin-F	ACTCTTCCAGCCTTCCTTC
β-actin-R	ATCTCCTTCTGCATCCTGTC
Nrf2-F	TCAGCGACGGAAAGAGTATGA
Nrf2-R	CCACTGGTTTCTGACTGGATGT

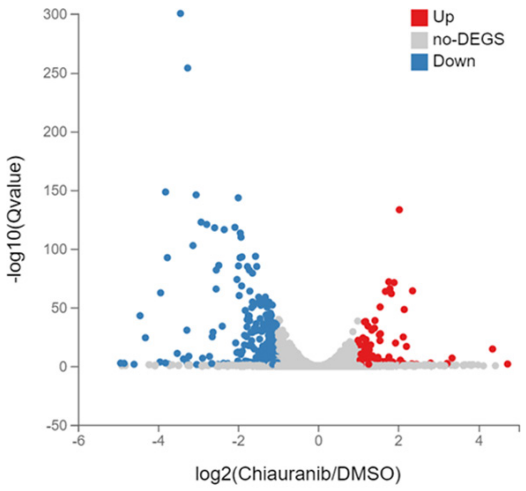

Supplementary Figure 1. Volcanic map of DEGs between DMSO and Chiauranib groups. DEGs between DMSO and Chiauranib groups were displayed by volcanic map. The X-axis represented the difference multiples after log2 conversion, and the Y-axis represented the significant value after log10 conversion. The blue one represented down-regulated DEGs, the red one represented up-regulated DEGs, and the gray one represented non-DEG. $\log_2|FC| \geq 1$ and $P < 0.05$.

GSEA:DMSO vs Chiauranib

Rank	Hallmark name	NES	p-value
1	Oxidative phosphorylation	1.898	0.000
2	Drug metabolism - cytochrome P450	1.807	0.001
3	p53 signaling pathway	1.750	0.002
4	Lysosome	1.729	0.000
5	Hedgehog signaling pathway	1.670	0.006
6	Proteasome	1.670	0.006
7	Antigen processing and presentation	1.653	0.004
8	Glycosphingolipid biosynthesis - ganglio series	1.584	0.020
9	N-Glycan biosynthesis	1.567	0.010
10	Arachidonic acid metabolism	1.544	0.016

Supplementary Figure 2. Gene set enrichment analysis (GSEA) of DEGs DMSO and Chiauranib groups. The significantly enriched hallmark pathways in GSEA were listed.

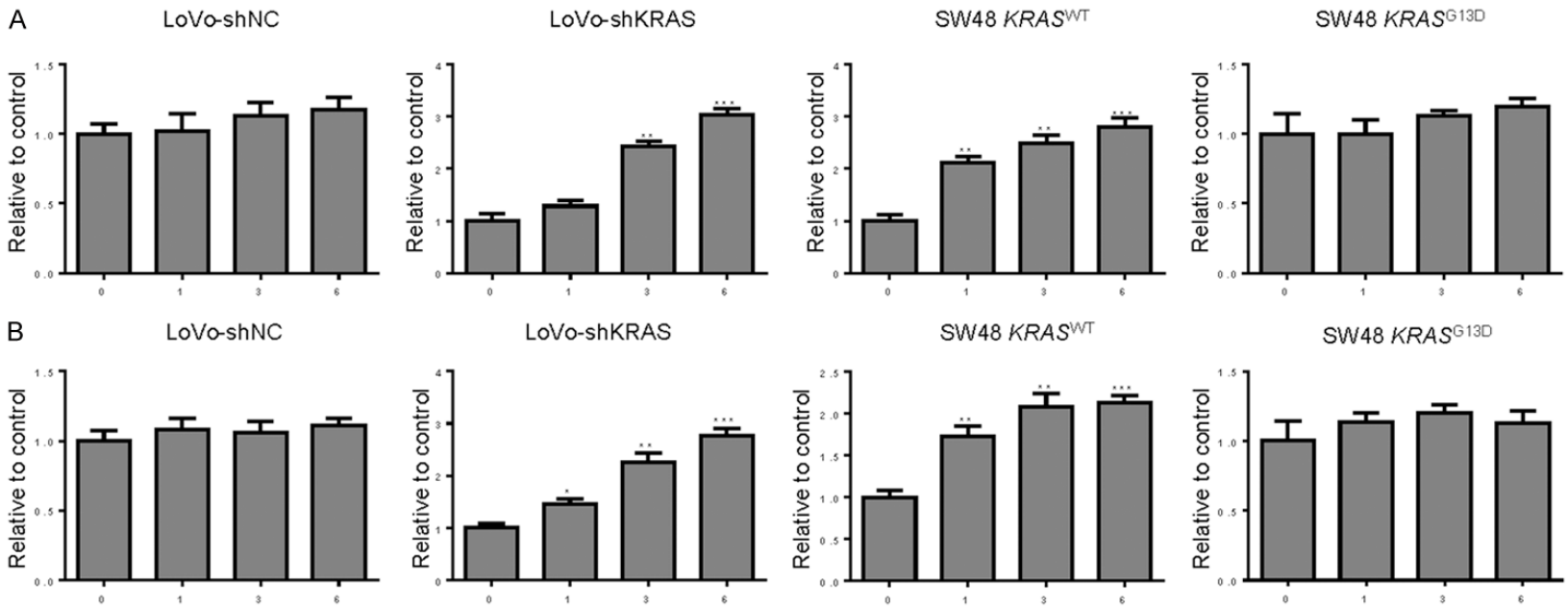

Supplementary Figure 3. Statistical analysis of ROS levels in CRC cells after treatment with Chiauranib. (A, B) Statistical analysis of (A) mitochondrial $O_2^{\bullet-}$ and (B) H_2O_2 in *KRAS*^{WT} SW48, *KRAS*^{G13D} SW48, LoVo-shNC and LoVo-shKRAS cells. Bars represented the mean ± SD of three independent experiments; **P* < 0.05, ***P* < 0.01 and ****P* < 0.001.

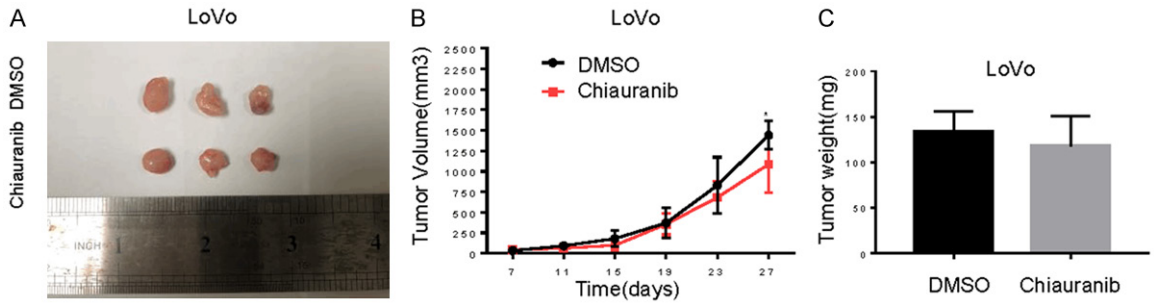

Supplementary Figure 4. The antitumor effects of Chiauranib in LoVo Xenograft Models. (A-C) (A) The representative morphology, (B) tumor growth rate, and (C) tumor weight were shown as a result of treatment with Chiauranib (40 mg/kg) once every three days in LoVo Xenograft Models. Data are shown as mean ± SD; *$P < 0.05$.

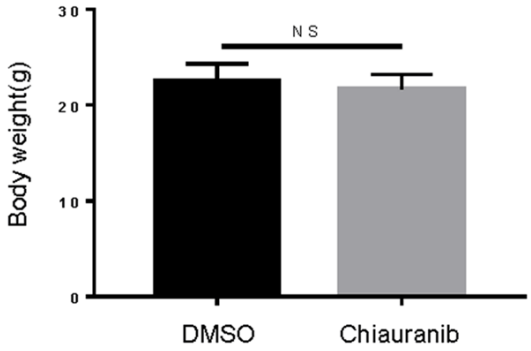

Supplementary Figure 5. The body weight of SW48 Xenograft mice between DMSO and Chiauranib groups. The body weight of SW48 Xenograft mice was measured at 27 days after inoculation.